Bioorganic & Medicinal Chemistry xxx (2016) xxx–xxx

Contents lists available at ScienceDirect

Bioorganic & Medicinal Chemistry

journal homepage: www.elsevier.com/locate/bmc

Quinoxalinone (Part II). Discovery of (*Z*)-3-(2-(pyridin-4-yl)vinyl) quinoxalinone derivates as potent VEGFR-2 kinase inhibitors ☆

Leilei Shi [a], Jianfeng Zhou [b], Jifeng Wu [c], Junya Cao [d], Yuemao Shen [a], Hua Zhou [e], Xun Li [a,*]

[a] School of Pharmaceutical Sciences, Key Laboratory of Chemistry and Chemical Biology (Ministry of Education), Shandong University, Ji'nan, Shandong 250012, PR China
[b] School of Medicine and Pharmacy, Ocean University of China, Qingdao 266100, PR China
[c] Institute of Criminal Science and Technology, Ji'nan Public Security Bureau, Ji'nan 250100, PR China
[d] School of Medicine, Shandong University, Ji'nan 250012, PR China
[e] Department of Chemistry, Texas A & M University, College Station, TX 77842, USA

ARTICLE INFO

Article history:
Received 12 January 2016
Revised 1 March 2016
Accepted 3 March 2016
Available online xxxx

Keywords:
VEGFR-2 inhibitor
Quinoxalinone derivates
Antiangiogenesis
Pyridyl motif
Activity evaluation

ABSTRACT

Inhibition of VEGFR-2 kinase has been highlighted as one of the well-defined strategies to suppress tumor growth via blockade of angiogenesis. Guided by the principles of bioisosteric replacement and pharmacophoric fragment migration, a series of novel quinoxalinone derivates were designed, synthesized and evaluated for their VEGFR-2 inhibitory potencies. Among them, compounds **7c**, **8b**, **8c**, **8e** and **10b** displayed antiangiogenic abilities via the in vitro tube formation assay (cellular level) and ex vivo rat aortic ring assay (tissue level) at a low concentration (0.1 μM). By means of in vivo zebrafish embryo model, two (*Z*)-3-(2-(pyridin-4-yl)vinyl)quinoxalinone derivates **8c** and **8e** showed significant antiangiogenesis effects, suggesting they have potentials to be developed into antiangiogenesis agents via further structural optimization. Moreover, these two compounds also demonstrated potent inhibition toward VEGFR-2 and B-raf kinases in a low concentration (1 μM). A possible interpretation of our evaluation result has been presented by a molecular docking study by docking representative compound **8c** with VEGFR-2.

1. Introduction

Abnormal angiogenesis plays a critical role in carcinogenesis and metastasis of tumors, and is also the necessary path through which tumor transition from benign to malignant. Among the identified angiogenic factors that are involved in tumor angiogenesis, vascular endothelial growth factor receptor-2 (VEGFR-2), also known as kinase insert domain receptor (KDR) for human and Flk-1 for murine, is believed to be the primary and the most pivotal regulator.[1] VEGFR-2 can drive angiogenesis through binding with its natural ligand VEGF, a known promoter of angiogenesis and selective mitogen mediating the mitogenic signaling of endothelial cells, resulting in the stimulation of downstream signaling cascades and some endothelial responses, such as vessel permeability increase and endothelial cell proliferation enhancing. Consequently, the blockage of the VEGF/VEGFR-2 mediated signaling transduction represents a promising strategy for antiangiogenic therapy in the treatment of carcinoma, especially for metastatic or advanced solid tumors.[2]

In the past decades, efforts on aiming at the interference of VEGF/VEGFR-2 have exploited numerous tumor angiogenesis inhibitors (TAIs) with high selectivity and inhibitory efficacies, such as the anti-VEGF monoclonal antibody Bevacizumab, and small-molecule inhibitors such as ATP-competitive antiangiogenic agents, as shown in Figure 1,[3] confirming the attractiveness of VEGFR-2 targeting inhibitors for cancer therapy.

From the binding modes of these small molecular inhibitors with VEGFR-2, several structural features are required for achieving a potent efficacy:[4] (i) *a basic skeletal structure* that contains at least one H-bond acceptor (N atom is preferred, followed by the O atom) so as to interact with the NH of Cys919, the key amino acid residue in the catalytic ATP-binding domain. Monocyclic ring compounds (e.g., pyridine and pyrimidine) and several 5–6- or 6–6-bicyclic heterocycles, including but not limited to quinazoline, quinoline, benzimidazole, and indolin-2-one motifs, are common chemotypes utilized as basic backbones; (ii) *a functional group* acting as pharmacophore (e.g., amide or urea) that possesses both H-bond acceptor and donor in order to bind with two crucial residues (Glu885 and Asp1046) in the DFG (Asp-Phe-Gly) motif,

☆ Part I has been reported in BMC (Ref. 6).

* Corresponding author.
E-mail address: tjulx2004@sdu.edu.cn (X. Li).

http://dx.doi.org/10.1016/j.bmc.2016.03.008
0968-0896/

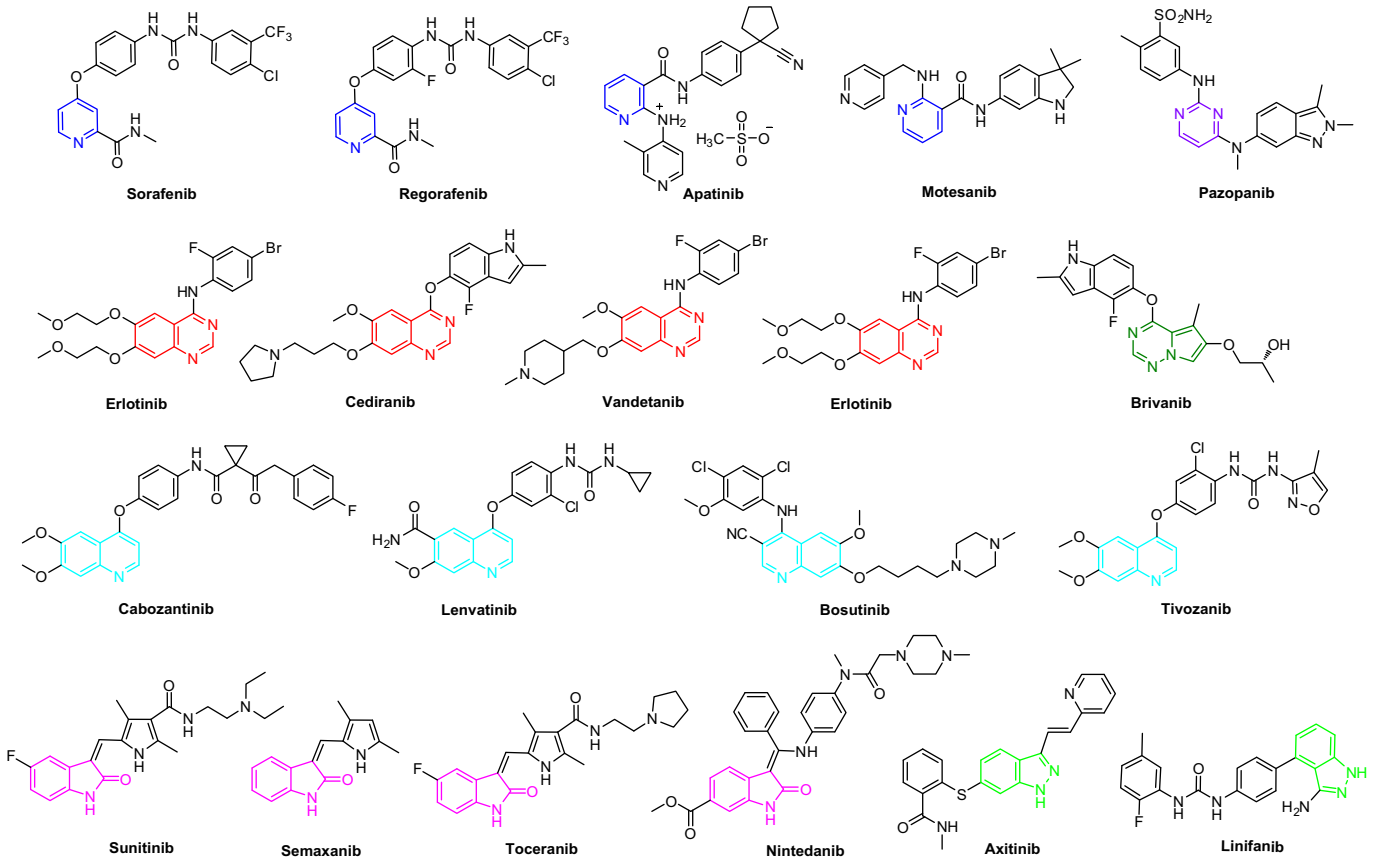

Figure 1. Representative VEGFR-2 inhibitors that have been approved or in various clinical trials.

an essential tripeptide sequence in the active kinase domain; (iii) *a hydrophobic substituent* that can embed into the deep cavity of hydrophobic pocket and further stabilizes the interaction between the inhibitor and target enzyme via hydrophobic *van der Waals* contact. All this binding information has provided guidance for developing novel VEGFR-2 tyrosine kinase inhibitors.

As a continuous work for quinoxalinone-derived medicinal chemistry in our lab,[5–7] the 6–6-bicyclic quinoxalinone (or quinoxalin-2-one) core, which contains both electron donor and acceptor, acts as a bioisostere with the validated scaffolding structures of several VEGFR-2 inhibitors, such as quinazoline (e.g., Vandetanib), quinoline (e.g., Cabozantinib), phthalazine (e.g., Vatalanib), and indoline-2,3-dione (e.g., Sunitinib), etc. It is therefore developed into new VEGFR-2 inhibitors as an attractive building block.

Axitinib (AG013736) is an approved VEGFR-2 inhibitor for renal cell carcinoma (RCC) with promising long-term safety profile[8] and inhibitory potency for BCR-ABL1-driven drug-resistant leukemia.[9] It has been proved that the conjugated pyridyl portion contributes to the solubility, metabolic stability, and pharmacokinetics.[10] The same pyridyl group can also be seen in Vatalanib (PTK787), another selective VEGFR-2 inhibitor which can sensitize multidrug resistant cancer cells to chemotherapy under hypoxic conditions and has entered phase III clinical trials as a second-line therapy in several types of metastatic or advanced cancers.[11–13] The pyridyl part contributes largely to the kinase selectivity in addition to solubility. This is because the pyridyl N can form pivotal H-bonding interaction with Lys1060, a residue of the kinase activation loop which plays an important role in selective recognition of the identified tyrosine kinase subtypes. In addition to this, Vatalanib doesn't form any other direct H-bonds with the ATP hinge region as most TAIs do, but rather occupies the hydrophobic areas of the enzyme using the central phthalazine scaffold as well as the terminal Cl-containing aryl moiety (Fig. 2). Moreover, a water-bridged indirect H-bond can be observed between the NH and Glu915/Cys917.[14]

On the basis of the structure–activity relationship (SAR) analysis of Axitinib and Vatalanib, it is reasonable to come to a conclusion that pyridyl, aryl and amide moieties are favorable contributors for selective VEGFR-2 inhibition. These pharmacophoric elements were therefore appropriately assembled in the quinoxalinone core so as to achieve potent VEGFR-2 inhibition and also the molecular diversity for further SAR investigation: (i) incorporating a pyridyl motif (Part A) into 3-position of quinoxalinone core via an aldol condensation to build a conjugated system as Axitinib does; (ii) installing an amide (Part B) and substituted aryl moiety (Part C) to the 1-N of quinoxalinone via nucleophilic substitution to maintain a similar molecular orientation as Vatalanib does; (iii) introducing an adjacent phenyl ring that links with the 1-N of quinoxalinone and amide (Part D) to simulate the structural pattern of the VEGFR-2 inhibitor Sorafenib and afford possible π–π stacking interaction with Phe1047 in the DFG area, as Sorafenib does;[15] (iv) hydrophobic substituents (R) were fixed at various positions of terminal aryl portion so as to penetrate into the extended hydrophobic pocket of the kinase domain of VEGFR-2.

To test our designing hypothesis, these quinoxalinone derivates were consequently subjected to the in vitro and in vivo antiangiogenesis evaluation. It resulted that compounds **8b**, **8c**, **8e**, **10b** were promising inhibitors against VEGFR-2 and might be viewed as potential leads for further structural modification. Preliminary SAR investigation and molecular modeling study of these derivatives were also discussed.

Please cite this article in press as: Shi, L.; et al. *Bioorg. Med. Chem.* (2016), http://dx.doi.org/10.1016/j.bmc.2016.03.008

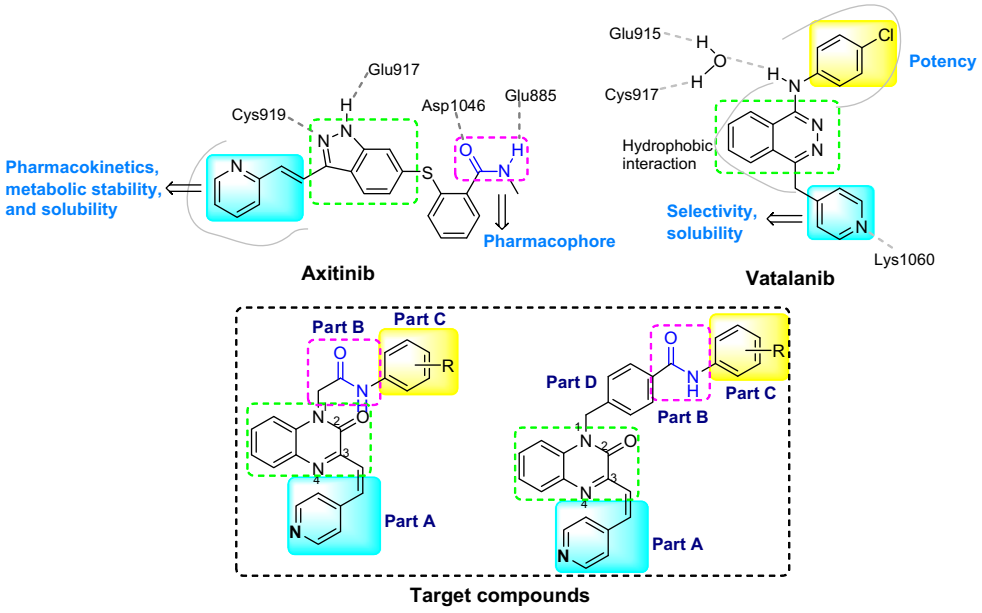

Figure 2. The design concepts of targeted compounds.

2. Results and discussion

2.1. Synthesis

To achieve the target quinoxalinone derivates **7**–**10**, the general synthetic steps outlined in Scheme 1 were adopted. Briefly, the condensation of the commercially available *o*-phenylenediamine **1** with ethyl pyruvate led to the formation of quinoxalinone core **2**. Owing to the keto–enol tautomerization of amide bond in quinoxalinone scaffold, subsequent nucleophilic substitution by using methyl 2-bromoacetate in the presence of K_2CO_3 provided a mixture of *N*-substituted ester compound **3** with relatively high yield (>50%)

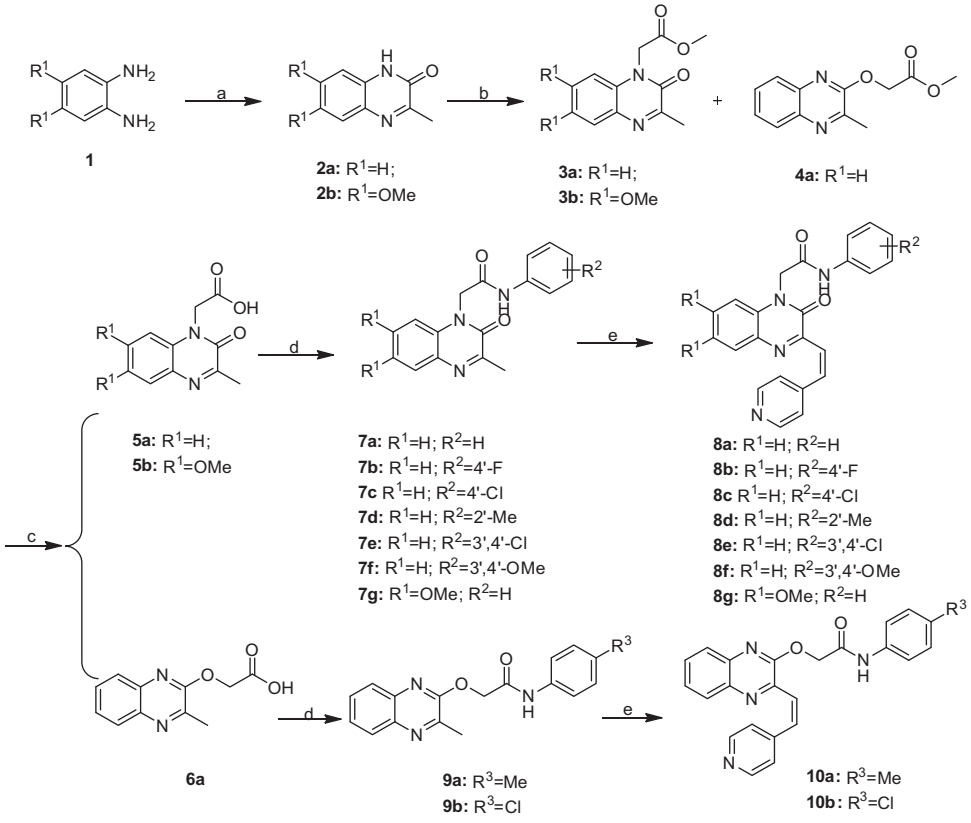

Scheme 1. General procedures for the synthesis of quinoxalinone derivates. Reagents and conditions: (a) Ethyl pyruvate, anhydrous EtOH, rt; (b) methyl bromoacetate, K_2CO_3, acetone, reflux; (c) LiOH, Dioxane/H_2O (3:1, v:v); (d) substituted aniline, isobutyl chloroformate, 4-methylmorpholine, anhydrous THF, 0 °C–rt; (e) 4-pyridinecarboxaldehyde, concentrated sulfuric acid, acetic acid, 50 °C.

Please cite this article in press as: Shi, L.; et al. *Bioorg. Med. Chem.* (2016), http://dx.doi.org/10.1016/j.bmc.2016.03.008

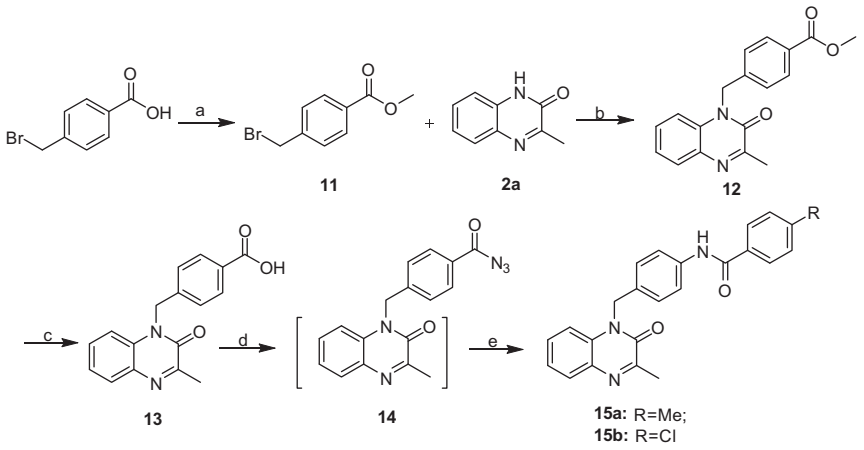

Scheme 2. Reagents and conditions: (a) acetyl chloride, anhydrous methanol, reflux; (b) K_2CO_3, KI, acetone, reflux; (c) KOH, anhydrous alcohol, H_2O, rt; (d) DPPA, dioxane, TEA, reflux; (e) substituted anilines, TEA, rt.

and the *O*-substituted ester compounds **4** with relatively low yield (<30%). After purification by column chromatography method, the separated ester compounds were respectively submitted to the following hydrolization under basic condition to give the corresponding carboxylic acids **5** and **6**. This was followed by coupling with various anilines in the existence of isobutyl chloroformate and *N*-methylmorpholine (NMM) in anhydrous THF to afford the quinoxalinone amides **7** and **9**. In this reaction, apart from THF, other aprotic polar solvents such as dichloromethane (CH_2Cl_2) and *N*,*N*-dimethylformamide (DMF) are possible alternatives. Treatment of quinoxalinone amides **7** or **9** with 4-pyridinecarboxaldehyde using a small amount of concentrated sulfuric acid as catalyst via an aldol condensation furnished the final products **8** and **10**. In these two final products, the coupling constants for the vinyl protons (J = 5.1 Hz) clearly indicate that double bonds is *cis*-configuration.

The synthesis of compounds **15a** and **15b** is illustrated in Scheme 2. Nucleophilic substitution of quinoxalinone core **2a** with methyl 4-(bromomethyl)benzoate (**11**), which was obtained via esterification of the commercially available 4-(bromomethyl)benzoic acid, gave the ester compound **12**. The subsequent ester hydrolization led to the carboxylic acid **13**, which was subjected to the treatment of diphenylphosphoryl azide (DPPA) and was converted to the acyl azide **14**. The intermediate was treated in situ with anilines via nucleophilic substitution to yield the amide compounds **15**.

Actually, our original intention is to introduce the diaryl urea functionality, a well-defined pharmacophoric moiety in VEGFR-2 inhibitors by forming essential H-bonding interactions with DFG motif of VEGFR-2,[16,17] to 1-N position of quinoxalinone core to further explore the SAR. However, in our synthetic condition as shown in Scheme 2, when the carboxylic acid **13** worked with DPPA, the azido-substituted intermediate **14** rather than our assumed isocyanate was obtained. The possible reason might be that the reaction temperature is not high enough using dioxane as solvent. Based on this, the diaryl urea derivatives are underway in our lab and the results will be reported later.

2.2. Biological evaluation

2.2.1. Antiproliferation assay

Considering VEGFR-2-targeted inhibitors are inherently cytostatic agents that can only delay tumor growth via inhibition of newly formed blood vessels but not completely eliminate tumor cells as traditional cytotoxic agents (chemotherapeutics) do, target compounds **7b**, **7c**, **8a**–**8g**, **9**, **10**, and **15** were initially submitted to the cytotoxic evaluation against a panel of human tumor cell lines by MTT assay, which was performed in triplicates. As summarized in Table 1, all the tested compounds displayed no or weak cytotoxic effects against six kinds of tumor cells, MCF-7 (breast carcinoma), 3AO (ovarian carcinoma), PC-3 (prostatic carcinoma), K562 (human chronic myeloid leukemia), HepG-2 (hepatic carcinoma) and Hela (cervix adenocarcinoma) under the testing conditions, as compared with the approved VEGFR-2 inhibitor Pazopanib (GW786034). In this regard, the target compounds are proved to be potentially cytostatic rather than cytotoxic agents.

2.2.2. In vitro antiangiogenic ability in a tube formation assay

Given tube formation of vascular endothelial cells is an important process during tumor angiogenesis, and human umbilical vein endothelial cells (HUVECs) can form capillary-like structures in the presence of Matrigel under the stimulation of VEGF to simulate the tumor angiogenetic process, the transmutation of HUVECs in Matrigel is thereby utilized as a validated in vitro model to evaluate the antiangiogenic ability. Compounds **7b**, **7c**, **8a**–**8g**, **9**, **10** and **15** were subsequently submitted to the tube formation inhibitory assay, using Pazopanib as a positive control. As shown in Figure 3, five compounds **7c**, **8b**, **8c**, **8e** and **10b** were effectively inhibited VEGF-induced tube formation of HUVECs in a dose-dependent manner.

2.2.3. Ex vivo antiangiogenic ability in rat aortic ring

Rat aortic ring microvessel growth is another practical and cost effective assay of angiogenesis, which offers an intuitive observation of the ex vivo antiangiogenic effect and bridges the gap between in vitro and in vivo models. By using intact vascular explants that were cultured in collagen gel, the rat aortic ring model can reproduce the microvascular networks more accurately in which angiogenesis can take place rather than those with isolated endothelial cells. The assay results demonstrated that five compounds, **7c**, **8b**, **8c**, **8e** and **10b**, with anti-angiogenetic activities at the cellular level, also had capacities to inhibit microvessel sprouting in the mimetic angiogenic process at the tissue level under the experimental conditions. As evinced in Figure 4, the antiangiogenic effects of five test compounds were even better than that exerted by the reference Pazopanib at the same concentrations.

2.2.4. In vivo antiangiogenic ability in zebrafish model

The ideal animal model to evaluate the antiangiogenesis effect should provide easily visible blood vessels growing in their natural

Table 1
The anti-proliferative results of target compounds

Compds/cell lines	MCF-7[a] (IC_{50}/μM)	3AO[a] (IC_{50}/μM)	PC-3[a] (IC_{50}/μM)	K562[a] (IC_{50}/μM)	Hela[a] (IC_{50}/μM)	BEAS-2B[a] (IC_{50}/μM)
7b	>100	>100	>100	>100	55.45 ± 2.31	>100
7c	>100	40.23 ± 1.92**	>100	>100	>100	>100
8a	>100	>100	>100	55.52 ± 3.11***	>100	>100
8b	49.04 ± 1.18***	>100	59.93 ± 1.75	>100	>100	>100
8c	>100	>100	>100	50.44 ± 2.45***	>100	>100
8d	>100	69.65 ± 0.32***	>100	>100	>100	>100
8e	47.57 ± 2.47***	>100	>100	>100	>100	>100
8f	>100	>100	>100	55.23 ± 0.14***	>100	>100
8g	>100	55.65 ± 3.09*	>100	>100	>100	>100
9a	>100	>100	>100	>100	74.56 ± 0.21	>100
9b	>100	>100	68.05 ± 2.11	>100	>100	>100
10a	60.22 ± 1.44***	>100	>100	>100	>100	>100
10b	>100	>100	>100	49.86 ± 3.45***	>100	>100
15a	>100	>100	>100	>100	>100	>100
15b	47.57 ± 4.47***	>100	39.56 ± 0.23	>100	>100	>100
Pazopanib	76.78 ± 0.019	50.23 ± 0.98	>100	89.32 ± 0.23	>100	>100

[a] Results are presented as the mean ± SD for at least three experiments for each group.
* P <0.05.
** P <0.01.
*** P <0.001.

environment, and rapid responses of live organism to drugs, allowing rapid screening of the test compounds.[18] In this context, the in vivo vascular studies of the compounds **7c**, **8b**, **8c**, **8e** and **10b** were further submitted to the anti-angiogenetic evaluation on a well-accepted vertebrate zebrafish (*Danio rerio*) embryos model, using vatalanib as the positive control.

To attain an optimal visualization, the Tg(*flk1*:GFP) transgenic zebrafish embryos expressing enhanced green fluorescent protein (GFP) in their endothelial cells under the control of *flk1*/*VEGFR-2* promoter was used in the assay, with a clear view of vasculature under the fluorescence microscopy.[19] The main vascular structures of zebrafish embryos include the dorsal longitudinal anastomotic vessel (DLAV), posterior cardinal vein (PCV), dorsal aorta (DA) and intersegmental vessel (ISV), as manifested in Figure 5. The anti-angiogenic effect was assessed according to the inhibitory effects of different doses of test compounds on ISV formation in the zebrafish embryos. In this study, after post-fertilization of zebrafish embryos at 24 h, and treated embryos with test compounds (**7c**, **8b**, **8c**, **8e** and **10b**) for 48 h, **8c** and **8e** showed significantly dose-dependent inhibition of ISV formation at the concentrations of 10, 50 and 100 μM, **10b** gave a moderate inhibitory effect, while **8b** presented a weak inhibition in comparison with the vehicle-treated control (0.2% DMSO). As for the positive control (vatalanib), the embryos displayed complete ISV regression at the concentration of 10 μM. As far as compound **7c** was concerned, ISV malformation was observed at 100 μM concentration. These data clearly demonstrated the anti-angiogenic property of target compounds, largely owing to the blood vessel inhibition rather than the toxicity of the existing vasculature.

2.2.5. Enzymatic inhibition assay

Compounds that revealing obvious antiangiogenic activities (**7c**, **8b**, **8c**, **8e** and **10b**) were further evaluated for their inhibitory efficacies on several kinases that involved in angiogenesis. In vitro enzymatic inhibition percentage (%) of compounds at 1 μM against recombinant human kinase insert domain receptor (KDR/VEGFR-2), serine/threonine protein kinase B-RAF, tyrosine kinases FGFR1 and EGFR were performed.[20] The levels of phosphorylation of the kinase-specific ligand peptides at 1 μM of compounds were measured, and the kinase inhibition profile was shown in Table 2. Among them, compounds **8e**, **8c**, **10b** displayed the most potent inhibition toward VEGFR-2 in a low concentration (1 μM), followed by the **7c**, and **8b** gave the least potency, which were consistent with that of their in vitro and in vivo activities. Moreover, all the test compounds exhibited weaker activities than the reference standards (staurosporine and sorafenib), however, they displayed selective inhibition against VEGFR-2 as compared with other angiogenesis-related kinases. It is worth mentioning that compounds **8c**, **8e** and **10b**, in addition to exerting VEGFR-2 inhibition, also displayed partly inhibitory abilities towards B-RAF, another critical kinase in mediating tumor proliferation and angiogenesis, and also has close correlation with tumor multidrug resistance (MDR).[21] As a result, these analogues might be expected to develop into multi-targeted anti-tumor agents after further chemical optimization.

2.3. Structure–activity relationships (SARs)

Collectively, the in vitro and in vivo results supported an important role of the introduced pyridyl, amide and aryl motifs, which have been validated as pharmacophoric structures and favorable contributors for selective VEGFR-2 inhibition. Typically, when amide and aryl substituents were present at 1-N position of the quinoxalinone skeleton, compounds **8a–g**, to a greater extent, generated most potent VEGFR-2 inhibition, in comparison with compound **7** (without pyridyl motif), or compounds **9** and **10**, in which the amide aryl substituents were present at 2-O position of the quinoxalinone skeleton. However, in the cases of compounds **15a** and **15b**, the introduction additional phenyl ring between quinoxalinone core and amide functionality did not exert an expected improved potency, but a total loss of activity. This might be derived from the less effectiveness of biphenyl amide structure, as compared with the diaryl urea functionality which has been recognized as an critical pharmacophore in designing potential VEGFR-2 inhibitors.[22]

Comparing with the impacts of substituents on quinoxalinone core, we can conclude that introducing substituent (e.g., methoxyl) to the quinoxalinone core is unfavorable for the bioactivity. Next, we examined the impact of the hydrophobic substituent variations on the terminal phenyl ring on their bioactivities. Considering methyl and halogen groups in *meta*- and/or *para*-position are the most frequent substitution pattern in type II VEGFR-2 inhibitors,[23] five groups (H, F, Cl, CH_3, OCH_3) are investigated in our target compounds **7**, **8** and **10**. As a consequence, compounds **7c**, **8b**, **8c**, **8e**

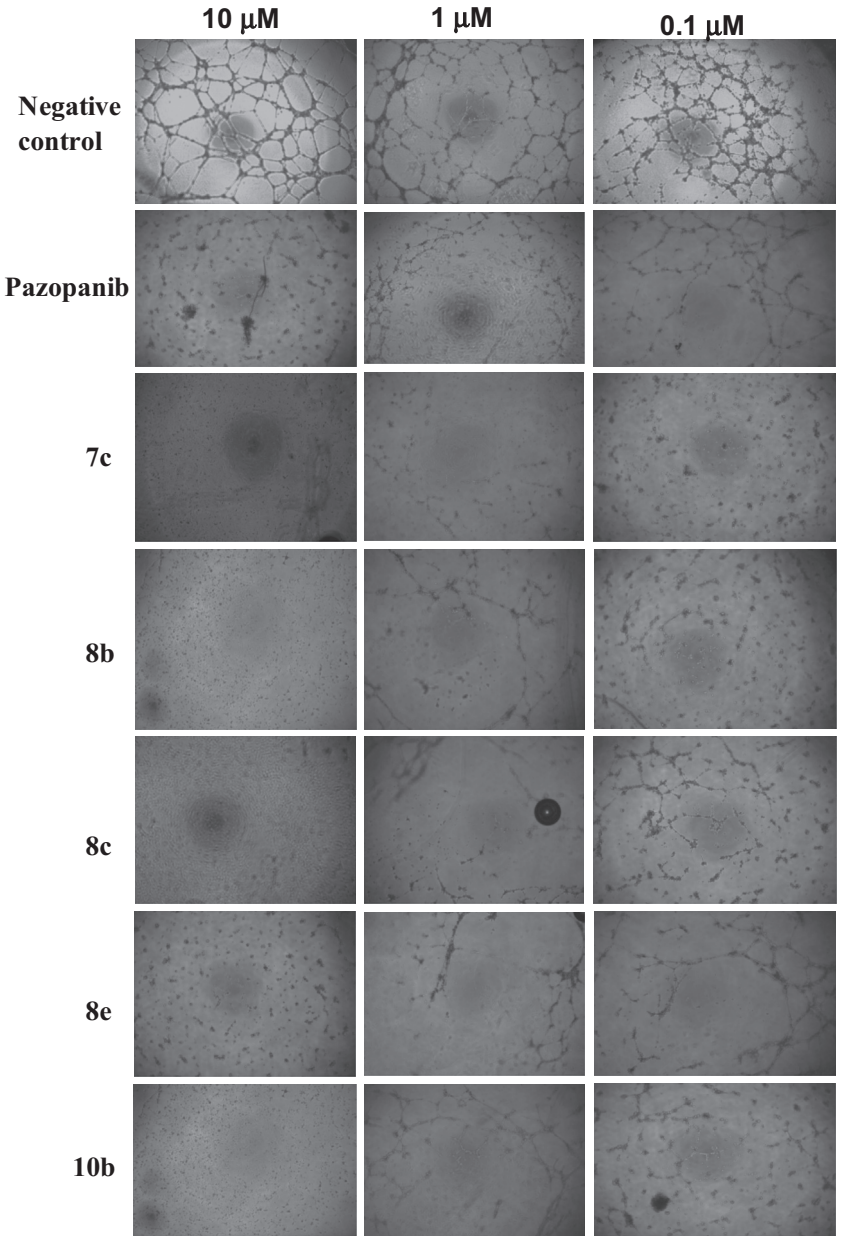

Figure 3. Anti-angiogenesis assay results on HUVEC.

and **10b** presented similar anti-angiogenetic bioactivity, implying the halogen-substitution is the most preferred substitutions against VEGFR-2. And else, different halogens in aromatic ring have similar levels of impacts on their bioactivities. We envisioned that the small halogens might provide an effective binding interaction with amino acid residues in target protein, leading to a favorable occupation into the hydrophobic pocket. Additionally, activity of substitution in *para*-position is better than *meta*-position.

2.4. Molecular docking study

To gain insight into the binding pattern of these compounds, one of the active VEGFR-2 inhibitors, **8c**, was chosen to dock into the active site of VEGFR-2 tyrosine kinase (PDB ID: 3EWH) using Autodock program. The resulting optimal binding mode of **8c**, as exhibited in Figure 6, unraveled several favorable interactions: (i) the N atom of pyridyl motif, acting as a hydrogen bond acceptor, interacts with the key Cys917 residue with distance of 1.87 Å; (ii) the introduced carbonyl O of amide functionality acts as a hydrogen bond acceptor to interact with Lys866 with distance of 1.63 Å; (iii) the *para*-Cl on the terminal phenyl ring orients this moiety to penetrate deeply into hydrophobic pocket of enzyme by forming two hydrogen bonds with Asp1026 and Asn1031, with distances of 2.10 Å and 2.22 Å, respectively, and (iv) the formation of non-covalent π–π stacking interaction between the aromatic quinoxalinone core and Phe1045 further stabilizes the binding interactions. Based on these docking information, the (*Z*)-3-(2-(pyridin-4-yl)vinyl)quinoxalinone structure can be regarded as a favorable motif for new inhibitor design owing to its contribution to effective hinge-binding interaction.

3. Conclusion

In summary, we report the design, synthesis, and biological evaluation of novel (*Z*)-3-(2-(pyridin-4-yl)vinyl)quinoxalinone derivatives as a new class of VEGFR-2 kinase inhibitors. SAR

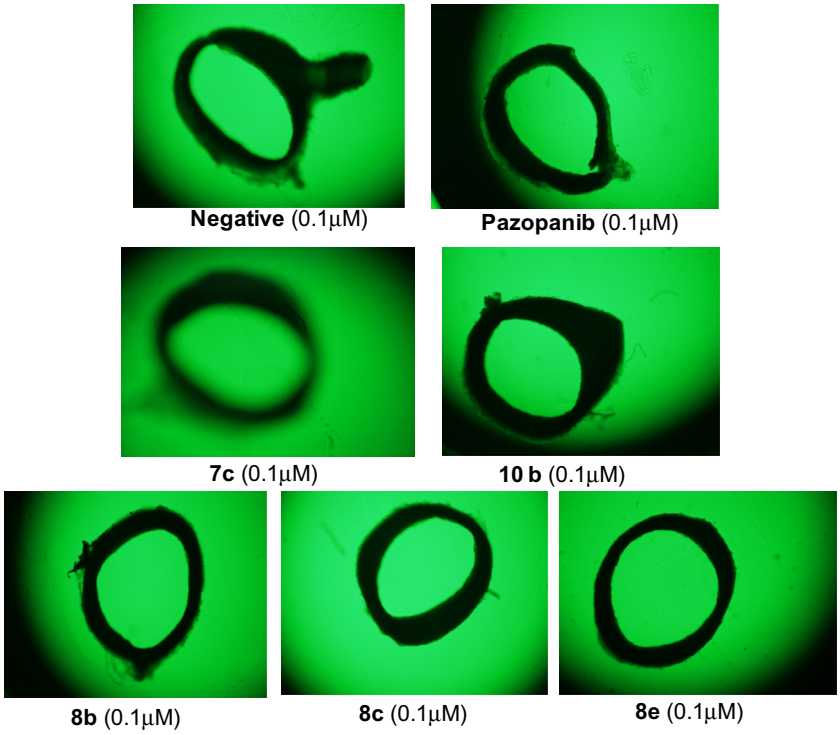

Figure 4. Anti-angiogenesis assay results on arterial ring of rat.

investigations manifested that this novel skeletal structure was tolerable to the introduction of favorable contributors for selective VEGFR-2 inhibition, such as pyridyl and amide moieties, leading to moderate to improved potencies. These derivatives did not exert cytotoxic effect. However, compounds **7c**, **8b**, **8c**, **8e** and **10b** clearly exhibited anti-angiogenesis effects in in vitro anti-angiogenetic assessment via both HUVEC tube formation assay and ex vivo rat aortic ring assay. Among these four compounds, **8b**, **8c**, **8e** and **10b** were withstood the in vivo test in zebrafish embryos model. Further kinase inhibition screening proved that although the inhibitory potencies of all of tested inhibitors did not surpass the reference standard, they exerted considerable selectivity profiling against other angiogenesis-related kinases, such as EGFR and FGFR1. Three test compounds, **8c**, **8e** and **10b**, presented clear inhibition percentage against VEGFR-2 in a low concentration (1 μM) and moderate inhibition toward B-Raf. Molecular modeling studies suggested that the inhibitor adopt several similar H-binding interactions as the designing prototype (axitinib and vatalanib) do, the newly presented π–π stacking interaction also contributes to the binding conformation.[24,25] Overall, we envisioned that **8c**, **8e** and **10b** might be promising candidates to be considered for further chemical optimization.

4. Experimental section

4.1. Chemistry

4.1.1. General

All the starting materials including reagents and solvents, unless otherwise specified, were analytically pure and obtained from commercial suppliers. They were used without further purification and, when necessary, were purified and dried by standard protocols. All reactions except those in aqueous media were carried out by standard techniques for the exclusion of moisture. All reaction progress was monitored by thin-layer chromatography (TLC) on 0.25-mm silica gel plates (grade 60, GF_{254}) and visualized with UV light (254 nm), or iodine vapor. Flash chromatography was performed on silica gel (Qingdao Haiyang Inc., 300–400 mesh). Melting points were determined using X-6 digital display binocular microscope (uncorrected). If not specified, ^{1}H NMR and ^{13}C NMR spectra were recorded on a Bruker Advance DRX-600 using $CDCl_3$ or DMSO-d_6 as solvents. If it has been indicated as 400 MHz or 300 MHz, AVANCEII-400 or AVANCEII-300 spectrometer were employed, and TMS as an internal standard. Chemical shift values (δ) are reported in parts per million (ppm) and coupling constants (J) are given in hertz (Hz), and splitting patterns are designated as follows: s, single; d, doublet; t, triplet; q, quartet; m, multiplet. Elemental analyses were carried out on a Perkin–Elmer C, H, N elemental analyzer. Electrospray ionization mass spectrometry (ESI-MS) data were collected on a Micromass Qtof-Micro LC–MS instrument.

4.1.2. General synthetic procedure for the preparation of 3-methylquinoxalin-2(1*H*)-one (2)

o-Phenylenediamine (0.02 mol, 2.16 g) was suspended in anhydrous ethanol (20 mL). The mixture was then cooled in an ice bath. A solution of ethyl pyruvate (0.022 mol, 25.52 g) in anhydrous ethanol (5 mL) was added dropwise over a period of 20 min under stirring. The resulting solution was allowed to react at room temperature for 6 h until the TLC showed the reaction has completed. The resulting precipitate was filtered and washed with anhydrous ethanol (2 × 5 mL), and dried in vacuum to give the product **2a** (3.04 g, 95%) as a white solid which was pure enough for further reaction. Mp: 241.0–242.7 °C; ESI-MS *m*/*z*: 161.6 $[M+H]^+$. Anal. Calcd for $C_9H_8N_2O$: C, 67.49; H, 5.03; N, 17.49; Found: C, 67.50; H, 5.05; N, 17.48.

For 6,7-dimethoxy-3-methylquinoxalin-2(1*H*)-one (**2b**): light brown powder, yield: 43%, ESI-MS *m*/*z*: 221.8 $[M+H]^+$. Mp: 261.0–262.0 °C. Anal. Calcd for $C_{11}H_{12}N_2O_3$: C, 59.99; H, 5.49; N, 12.72; Found: C, 60.01; H, 5.47; N, 12.74.

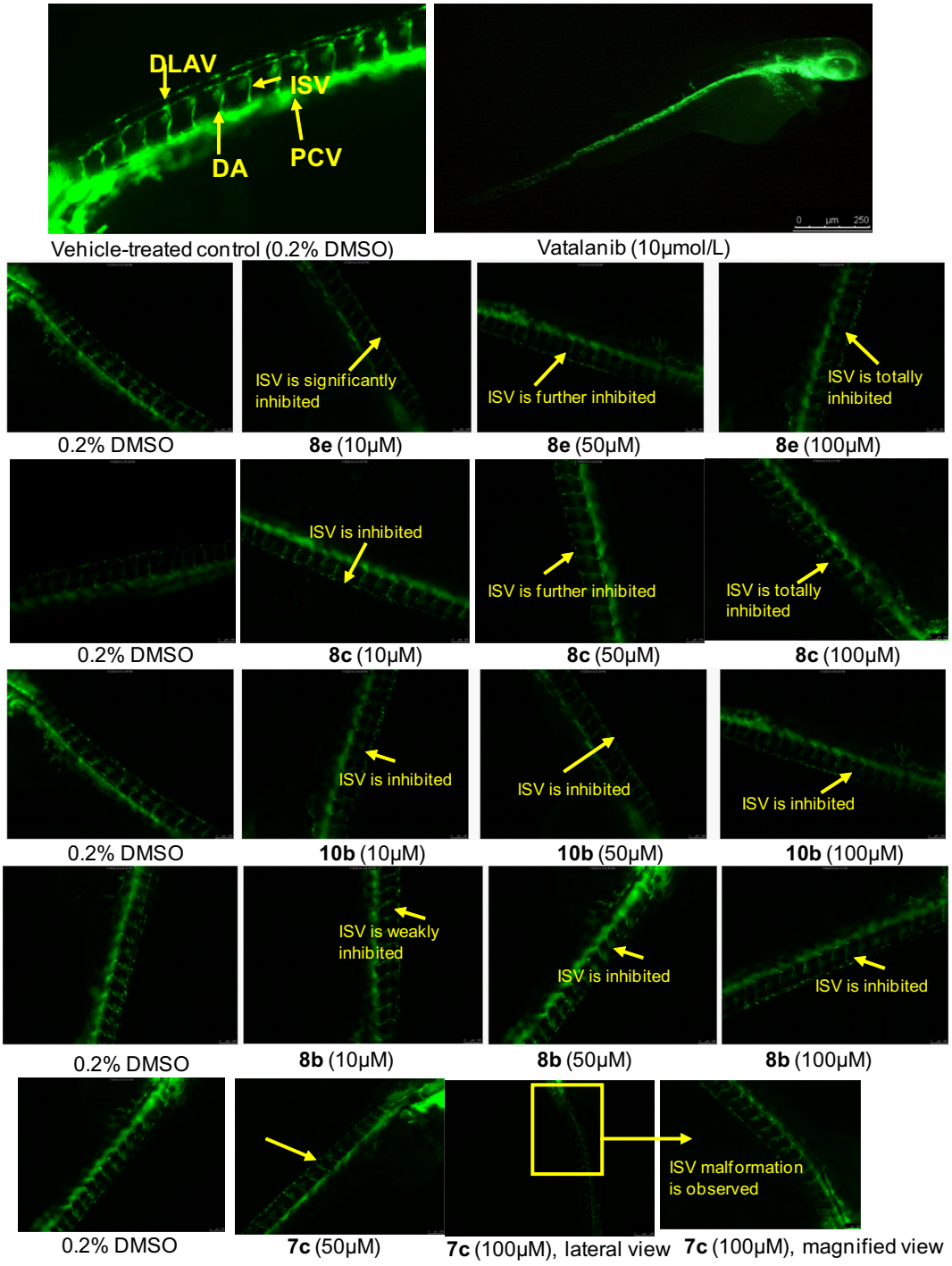

Figure 5. Anti-angiogenic activities of target compounds using zebrafish model.

Table 2
Kinase inhibitory activities of (*Z*)-3-(2-(pyridin-4-yl)vinyl)quinoxalinone derivates

Comps (1 μM)	VEGFR-2 (% inhibition) [a]	EGFR (% inhibition) [a]	B-RAF (% inhibition) [a]	FGFR1 (% inhibition) [a]
7c	19	1	8	0
8b	6	0	4	2
8c	44	2	25	5
8e	56	7	20	8
10b	37	0	17	0
Staurosporine	82	70	–	–
Sorafenib	90	–	58	–

[a] Results are given as average inhibitory values.

Please cite this article in press as: Shi, L.; et al. *Bioorg. Med. Chem.* (2016), http://dx.doi.org/10.1016/j.bmc.2016.03.008

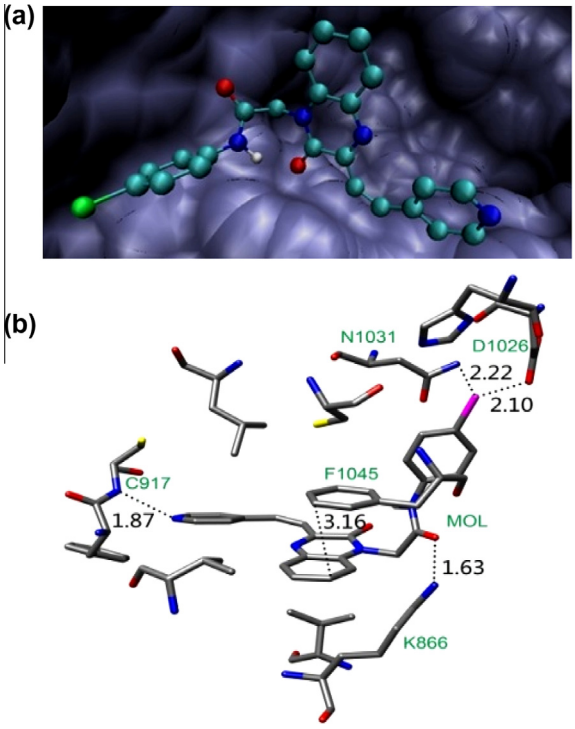

Figure 6. (a) Molecular docking result of compound **8c** with VEGFR-2 (PDB entry: 3EWH). (b) The observed interactions between **8c** and target enzyme shown by LIGPLOT.

4.1.3. General procedure for methyl 2-(3-methyl-2-oxoquinoxalin-1(2*H*)-yl)acetate (3)

Compound **2a** (10 mmol, 1.6 g), K_2CO_3 (12 mmol, 1.66 g) and KI (1 mmol, 0.17 g) were suspended in anhydrous acetone (15 mL) at 0 °C. Then a solution of methyl bromoacetate (12 mmol, 1.84 g) in anhydrous acetone (10 mL) was added dropwise into the above mixture. The resulting mixture was then stirred on oil bath at 62 °C for 8 h under nitrogen atmosphere. After completion of reaction, the solvent was removed under vacuum and the residue was partitioned between EtOAc (30 mL) and distilled water (10 mL). The organic layer was separated and washed with brine (2 × 15 mL), dried over anhydrous $MgSO_4$, filtered, and concentrated in vacuo to afford the crude product, which was further purified by silica gel flash chromatography (PE:EA = 8:1, v:v) to furnish 1.28 g of **3a** as a white solid, yield 52%. Mp: 120.0–121.1 °C, ESI-MS *m*/*z*: 247.1 $[M+H]^+$; ^1H NMR: ($CDCl_3$, ppm) δ: 7.05–7.86 (m, 4H, ArH), 5.05 (s, 2H, $NCH_2C{=}O$), 3.18 (s, 3H, OCH_3), 2.62 (s, 3H, $N{=}CCH_3$). Anal. Calcd for $C_{12}H_{12}N_2O_3$: C, 62.06; H, 5.21; N, 12.06; Found: C, 62.07; H, 5.22; N, 12.04.

For methyl 2-(6,7-dimethoxy-3-methyl-2-oxoquinoxalin-1(2*H*)-yl)acetate (**3b**): 47%, light yellow solid, mp 144–145 °C, ESI-MS *m*/*z*: 291.6 $[M-H]^-$. Anal. Calcd for $C_{14}H_{16}N_2O_5$: C, 57.53; H, 5.52; N, 9.58; Found: C, 57.52; H, 5.55; N, 9.57.

4.1.4. Methyl 2-((3-methylquinoxalin-2-yl)oxy)acetate (4a)

This compound was prepared from **2a** using the same experimental procedure as for **3**. Owing to the keto–enol tautomerization, the *O*-substituted ester compounds **4a** was isolated with relatively low yield (28 %) as a light yellow solid. ESI-MS *m*/*z*: 233.6 $[M+H]^+$. Anal. Calcd for $C_{12}H_{12}N_2O_3$: C, 62.06; H, 5.21; N, 12.06; Found: C, 62.07; H, 5.22; N, 12.07.

4.1.5. 2-(3-Methyl-2-oxoquinoxalin-1(2*H*)-yl)acetic acid (5)

Compound **3a** (20 mmol, 4.64 g) and KOH (2.24 g, 40 mmol) were suspended in 40 mL of dioxane and water (3:1, v:v), the resulting solution was allowed to react at room temperature for 3 h. The organic solvent was removed in vacuo and the resulting water phase was washed with EtOAc (2 × 10 mL), the combined water was acidified by 1 N HCl until white solid was precipitated. Filtered and recrystallized with 70% methanol to give the pure product **5a** (4.0 g, 92%) as a off-white solid. Mp: 225–226 °C, ESI-MS *m*/*z*: 217.5 $[M-H]^-$. Anal. Calcd for $C_{11}H_{10}N_2O_3$: C, 60.55; H, 4.62; N, 12.84; Found: C, 60.57; H, 4.63; N, 12.86.

For 2-(6,7-dimethoxy-3-methyl-2-oxoquinoxalin-1(2*H*)-yl) acetic acid **5b**: 87%, white solid, mp 233–234 °C, ESI-MS *m*/*z*: 277.6 $[M-H]^-$. Anal. Calcd for $C_{13}H_{14}N_2O_5$: C, 56.11; H, 5.07; N, 10.07; Found: C, 56.12; H, 5.06; N, 10.08.

4.1.6. 2-((3-Methylquinoxalin-2-yl)oxy)acetic acid (6a)

This compound was prepared from **4a** using the same experimental procedure as for **5**. It afforded 1.89 g (87%) of **6a** as light yellow solid, ESI-MS *m*/*z*: 217.3 $[M-H]^-$. Anal. Calcd for $C_{11}H_{10}N_2O_3$: C, 60.55; H, 4.62; N, 12.84; Found: C, 60.56; H, 4.64; N, 12.86.

4.1.7. General procedure for 2-(3-methyl-2-oxoquinoxalin-1(2*H*)-yl)-*N*-substituted phenylacetamide (7a–g)

A round-bottom flask charged with compound **5** (2 mmol) and 15 mL of anhydrous THF was successively added isobutyl chloroformate (2.4 mmol, 1.2 equiv), 4-methylmorpholine (2.4 mmol, 1.2 equiv) and stirred in an ice-salt baths for 30 min. Then the ice-salt bath was removed and appropriate aniline (2.4 mmol, 1.2 equiv) was added, the mixture was then allowed to react at room temperature under nitrogen atmosphere for about 4 h until the TLC showed the reaction has been completed. The reaction mixture was concentrated in vacuo and the resulting residue was extracted with ethyl acetate (3 × 50 mL), washed with water and dried over anhydrous $MgSO_4$. After filtration and concentration in vacuo, the obtained residue was purified by flash chromatography (PE/EtOAc = 4:1, v:v) to afford the desired products.

4.1.7.1. 2-(3-Methyl-2-oxoquinoxalin-1(2*H*)-yl)-*N*-phenylacetamide (7a). 1.22 g as white solid, yield: 81%; mp = 294–295 °C; ^1H NMR ($CDCl_3$): δ = 10.47 (s, 1H, ArNHC=O), 7.08–7.10 (m, 2H, ArH), 7.19–7.68 (m, 6H, ArH), 7.87–7.89 (d, *J* = 12.0 Hz, 1H, ArH), 5.02 (s, 2H, $NCH_2C{=}O$), 2.67 (s, 3H, $N{=}CCH_3$). ESI-MS *m*/*z*: 294.4 $[M+H]^+$. Anal. Calcd for $C_{17}H_{15}N_3O_2$: C, 69.61; H, 5.15; N, 14.33; Found: C, 69.62; H, 5.14; N, 14.34.

4.1.7.2. *N*-(4-Fluorophenyl)-2-(3-methyl-2-oxoquinoxalin-1(2*H*)-yl)acetamide (7b). 0.29 g as white solid, yield: 48%, mp = 280–281 °C; ^1H NMR (DMSO-d_6): δ = 10.50 (s, 1H, ArNHC=O), 7.80–7.813 (d, *J* = 7.8 Hz, 1H, ArH), 7.54–7.61 (m, 4H, ArH), 7.36–7.39 (m, 1H, ArH), 7.13–7.19 (m, 2H), 5.11 (s, 2H, $NCH_2C{=}O$), 2.47 (s, 3H, $N{=}CCH_3$). ESI-MS *m*/*z*: 312.4 $[M+H]^+$; 334.4 $[M+Na]^+$. Anal. Calcd for $C_{17}H_{14}FN_3O_2$: C, 65.59; H, 4.53; N, 13.50; Found: C, 65.60; H, 4.54; N, 13.48.

4.1.7.3. *N*-(4-Chlorophenyl)-2-(3-methyl-2-oxoquinoxalin-1(2*H*)-yl)acetamide (7c). 0.34 g as white solid, yield: 52%; mp = 267–268.5 °C; ^1H NMR (DMSO-d_6): δ = 10.56 (s, 1H, ArNHC=O), 7.81–7.8235 (d, *J* = 8.1 Hz, 1H, ArH), 7.61–7.62 (m, 2H, ArH), 7.48–7.59 (m, 2H, ArH), 7.34–7.40 (m, 3H, ArH), 5.12 (s, 2H, $NCH_2C{=}O$), 2.41 (s, 3H, $N{=}CCH_3$). ESI-MS *m*/*z*: 328.4 $[M+H]^+$; 350.4 $[M+Na]^+$; 366.7 $[M+K]^+$. Anal. Calcd for $C_{17}H_{14}ClN_3O_2$: C, 62.30; H, 4.31; N, 12.82; Found: C, 62.31; H, 4.32; N, 12.80.

4.1.7.4. 2-(3-Methyl-2-oxoquinoxalin-1(2*H*)-yl)-*N*-(*o*-tolyl)acetamide (7d). 2.22 g as white solid, yield: 77%; mp = 254–255 °C; ^1H NMR ($CDCl_3$): δ = 10.52 (s, 1H, ArNHC=O), 7.91–7.92 (d, *J* = 6.0 Hz, 1H, ArH), 7.22–7.39 (m, 3H, ArH), 7.02–7.18 (m,

4H), 5.04 (s, 2H, NCH_2C=O), 2.46 (s, 3H, N=CCH_3), 1.78 (s, 3H, $ArCH_3$). ESI-MS *m/z*: 308.5 $[M+H]^+$. Anal. Calcd for $C_{18}H_{17}N_3O_2$: C, 70.34; H, 5.58; N, 13.67; Found: C, 70.33; H, 5.59; N, 13.66.

4.1.7.5. *N*-(3,4-Dichlorophenyl)-2-(3-methyl-2-oxoquinoxalin-1(2*H*)-yl)acetamide (7e). 0.46 g as white solid, yield: 65%, mp = 274–274.5 °C, ^{1}H NMR (DMSO-d_6): δ = 10.74 (s, 1H, ArNHC=O), 7.93–7.933 (d, J = 1.8 Hz, 1H, ArH), 7.79 (dd, J_1 = 8.4 Hz, J_2 = 1.8 Hz, 1H, ArH), 7.59 (d, J = 8.4 Hz, 1H, ArH), 7.58 (dd, J_1 = 8.4 Hz, J_2 = 1.8 Hz, 1H, ArH), 7.50 (m, 2H, ArH), 7.38 (d, J = 8.4 Hz, 1H, ArH), 5.12 (s, 2H, NCH_2C=O), 2.47 (s, 3H, N=CCH_3). ESI-MS *m/z*: 362.3 $[M+H]^+$. Anal. Calcd for $C_{17}H_{13}Cl_2N_3O_2$: C, 56.37; H, 3.62; N, 11.60; Found: C, 56.38; H, 3.64; N, 11.59.

4.1.7.6. *N*-(3,4-Dimethoxyphenyl)-2-(3-methyl-2-oxoquinoxalin-1(2*H*)-yl)acetamide (7f). 0.39 g as white solid, yield: 56%, mp = 230–231 °C, ^{1}H NMR ($CDCl_3$): δ = 10.49 (s, 1H, ArNHC=O), 7.87–7.88 (d, J = 6.0 Hz, 1H, ArH), 7.21 (s, 1H, ArH), 7.07–7.17 (m, 3H, ArH), 7.04–7.043 (d, 1H, J = 1.8 Hz, ArH), 6.82–6.833 (d, 1H, J = 7.8 Hz, ArH), 4.99 (s, 2H, NCH_2C=O), 3.67 (s, 6H, 2 × OCH_3), 2.44 (s, 3H, N=CCH_3), ESI-MS *m/z*: 354.8 $[M+H]^+$. Anal. Calcd for $C_{19}H_{19}N_3O_4$: C, 64.58; H, 5.42; N, 11.89; Found: C, 64.59; H, 5.43; N, 11.88.

4.1.7.7. 2-(6,7-Dimethoxy-3-methyl-2-oxoquinoxalin-1(2*H*)-yl)-*N*-phenylacetamide (7g). 0.49 g as light yellow floccule, yield: 70%, mp = 257–258 °C, ^{1}H NMR (DMSO-d_6): δ = 10.42 (s, 1H, ArNHC=O), 7.57–7.583 (t, J = 7.8 Hz, 2H, ArH), 7.33–7.41 (m, 2H, ArH), 7.22–7.23 (s, 1H, ArH), 7.08–7.12 (dd, J_1 = J_2 = 12.0 Hz, 1H, ArH), 6.99 (s, 1H, ArH), 5.15 (s, 2H, NCH_2C=O), 3.77 (s, 6H, 2 × OCH_3), 2.47 (s, 3H, N=CCH_3). ESI-MS *m/z*: 354.5 $[M+H]^+$; 376.8 $[M+Na]^+$. Anal. Calcd for $C_{19}H_{19}N_3O_4$: C, 64.58; H, 5.42; N, 11.89; Found: C, 64.58; H, 5.44; N, 11.87.

4.1.8. General procedure for substituted (*Z*)-2-(2-oxo-3-(2-(pyridin-4-yl)vinyl)quinoxalin-1(2*H*)-yl)-*N*-substituted phenylacetamide (8a–g)

To a solution of compound **7a–g** (0.6 mmol) in acetic acid (15 mL) was added 4-pyridinecarboxaldehyde (0.72 mmol, 1.2 equiv) dropwise, and catalytic amount of concentrated sulfuric acid. The resulting solution was heated to 50 °C and reacted for 2 h until the completion of reaction via TLC. The reaction mixture was concentrated in vacuo and then water (15 mL) and ethyl acetate (30 mL) was added, the organic layers were separated and the water phase was basified by K_2CO_3 to pH to 7. The resulting water phase was extracted with ethyl acetate (50 mL), the combined organic phase was washed with water and dried over anhydrous $MgSO_4$. The obtained residue was purified by flash chromatography (PE/EtOAc = 3:1–1:3, v:v) to afford the desired products.

4.1.8.1. (*Z*)-2-(2-Oxo-3-(2-(pyridin-4-yl)vinyl)quinoxalin-1(2*H*)-yl)-*N*-phenylacetamide (8a). 0.89 g as white powder, yield: 71%; mp = 182–184 °C; ^{1}H NMR (400 MHz, DMSO-d_6): δ = 10.48 (s, 1H, ArNHC=O), 8.51–8.53 (m, 2H, ArH), 7.82–7.84 (d, J = 8.0 Hz, 1H, ArH), 7.57–7.60 (m, 3H, ArH), 7.52–7.5396 (d, J = 7.84 Hz, 1H, ArH), 7.40–7.4022 (d, J = 0.88 Hz, 2H, ArH), 7.31–7.36 (m, 3H, ArH), 7.07 (m, 1H, ArH), 5.65–5.6628 (d, J = 5.12 Hz, 1H, CH=C*H*Ar), 5.31–5.323 (d, J = 5.1 Hz, 1H, N=C—C*H*=CH), 5.16 (s, 2H, NCH_2C=O) ppm; ^{13}C NMR (100 MHz, DMSO-d_6): δ = 165.2, 157.7, 154.7, 154.6, 149.9, 139.1, 133.4, 132.4, 130.5, 129.6, 129.3, 124.1, 124.0, 121.5, 119.6, 115.2, 69.4, 45.7 ppm. ESI-MS *m/z*: 400.4 $[M+NH_4]^+$. Anal. Calcd for $C_{23}H_{18}N_4O_2$: C, 72.24; H, 4.74; N, 14.65; Found: C, 72.22; H, 4.75; N, 14.66.

4.1.8.2. (*Z*)-*N*-(4-Fluorophenyl)-2-(2-oxo-3-(2-(pyridin-4-yl)vinyl)quinoxalin-1(2*H*)-yl)acetamide (8b). White powder 0.18 g, yield 51%. Mp = 183–184 °C, ^{1}H NMR (300 MHz, DMSO-d_6): δ = 10.54 (s, 1H, ArNHC=O), 8.52–8.542 (d, J = 6.6 Hz, 2H, ArH), 7.81–7.843 (m, J = 9.9 Hz, 1H, ArH), 7.53–7.63 (m, 4H, ArH), 7.36–7.42 (m, 3H, ArH), 7.14–7.19 (m, 2H, ArH), 5.65–5.666 (d, J = 4.8 Hz, 1H, CH=C*H*Ar), 5.31–5.326 (d, J = 4.8 Hz, 1H, N=C—C*H*=CH), 5.14 (s, 2H, NCH_2C=O) ppm; ^{13}C NMR (75 MHz, DMSO-d_6): δ = 165.2, 159.8, 157.6, 154.7, 154.6, 149.9, 135.5, 133.4, 132.4, 130.5, 129.6, 124.0, 121.5, 121.4, 116.0, 115.8, 115.2, 45.7 ppm. ESI-MS *m/z*: 418.4 $[M+NH_4]^+$. Anal. Calcd for $C_{23}H_{17}FN_4O_2$: C, 68.99; H, 4.28; N, 13.99; Found: C, 69.00; H, 4.27; N, 14.01.

4.1.8.3. (*Z*)-*N*-(4-Chlorophenyl)-2-(2-oxo-3-(2-(pyridin-4-yl)vinyl)quinoxalin-1(2*H*)-yl)acetamide (8c). White powder 0.18 g (68%), mp = 205–206 °C, ^{1}H NMR (300 MHz, DMSO-d_6): δ = 10.64 (s, 1H, ArNHC=O), 8.52–8.5387 (d, J = 5.6 Hz, 2H, ArH), 7.78–7.81 (d, J = 9.0 Hz, 1H, ArH), 7.54–7.63 (m, 4H, ArH), 7.37–7.42 (m, 5H, ArH), 5.64–5.653 (d, J = 5.1 Hz, 1H, CH=C*H*Ar), 5.30–5.313 (d, J = 5.1 Hz, 1H, N=C—C*H* = CH), 5.15 (s, 2H, NCH_2C=O) ppm; ^{13}C NMR (75 MHz, DMSO-d_6): δ = 165.8, 154.7, 151.4, 150.8, 143.4, 139.2, 135.4, 133.1, 131.6, 131.3, 130.1, 126.9, 125.6, 124.6, 122.2, 120.9, 119.7, 115.5, 46.3 ppm, ESI-MS *m/z*: 436.7 $[M+NH_4]^+$. Anal. Calcd for $C_{23}H_{17}ClN_4O_2$: C, 66.27; H, 4.11; N, 13.44; Found: C, 66.28; H, 4.13; N, 13.42.

4.1.8.4. (*Z*)-2-(2-Oxo-3-(2-(pyridin-4-yl)vinyl)quinoxalin-1(2*H*)-yl)-*N*-(*o*-tolyl)acetamide (8d). White solid 1.48 g (77%), mp = 192–193 °C, ^{1}H NMR (400 MHz, DMSO-d_6): δ = 9.85 (s, 1H, ArNHC=O), 8.51–8.5247 (d, J = 5.88 Hz, 2H, ArH), 7.81–7.83 (d, J = 8.0 Hz, 1H, ArH), 7.59–7.63 (m, 2H, ArH), 7.36–7.51 (m, 4H, ArH), 7.07–7.23 (m, 3H, ArH), 5.63–5.643 (d, J = 5.1 Hz, 1H, CH = C*H*Ar), 5.31–5.323 (d, J = 5.1 Hz, 1H, N=C—C*H*N=CH), 5.20 (s, 2H, NCH_2C=O), 2.24 (s, 3H, $ArCH_3$) ppm; ^{13}C NMR (100 MHz, DMSO-d_6): δ = 165.4, 157.8, 154.8, 154.6, 149.9, 136.2, 133.3, 132.5, 132.3, 130.9, 130.4, 129.6, 126.5, 126.0, 125.3, 124.0, 121.5, 115.1, 69.4, 45.5, 18.3 ppm. ESI-MS *m/z*: 414.6 $[M+NH_4]^+$. Anal. Calcd for $C_{24}H_{20}N_4O_2$: C, 72.71; H, 5.08; N, 14.13; Found: C, 72.72; H, 5.07; N, 14.14.

4.1.8.5. (*Z*)-*N*-(3,4-Dichlorophenyl)-2-(2-oxo-3-(2-(pyridin-4-yl)vinyl)quinoxalin-1(2*H*)-yl)acetamide (8e). Yellow powder 0.48 g (56%); mp = 282–283 °C; ^{1}H NMR (400 MHz, DMSO-d_6): δ = 10.61 (s, 1H, ArNHC=O), 8.50–8.522 (d, J = 8.8 Hz, 2H, ArH), 7.82–7.8395 (d, J = 7.8 Hz, 1H, ArH), 7.51–7.61 (m, 4H, ArH), 7.36–7.41 (m, 5H, ArH), 5.61–5.6227 (d, J = 5.08 Hz, 1H, CHN=C*H*Ar), 5.31–5.3227 (J = 5.08 Hz, 1H, N=C—C*H* = CH), 5.14 (s, 2H, NCH_2C=O) ppm; ^{13}C NMR (100 MHz, DMSO-d_6): δ = 165.4, 157.6, 154.7, 154.6, 149.9, 138.1, 133.4, 132.4, 130.5, 129.6, 129.3, 127.6, 124.0, 121.5, 121.2.7, 115.2, 45.7 ppm. ESI-MS *m/z*: 451.5 $[M+H]^+$. Anal. Calcd for $C_{23}H_{16}Cl_2N_4O_2$: C, 61.21; H, 3.57; N, 12.41; Found: C, 61.22; H, 3.58; N, 12.43.

4.1.8.6. (*Z*)-*N*-(3,4-Dimethoxyphenyl)-2-(2-oxo-3-(2-(pyridin-4-yl)vinyl)quinoxalin-1(2*H*)-yl)acetamide (8f). Light yellow powder 0.62 g (70%); mp = 277–278 °C; ^{1}H NMR (400 MHz, DMSO-d_6): δ = 10.89 (s, 1H, ArNHC=O), 8.63–8.64 (d, J = 4.0 Hz, 2H, ArH), 8.03–8.07 (d, J = 16.0 Hz, 1H, ArH), 7.85–7.92 (m, 2H, ArH), 7.71–7.73 (m, 2H, ArH), 7.56–7.65 (m, 2H, ArH), 7.41–7.45 (m, 1H, ArH), 7.37–7.3755 (d, J = 2.2 Hz, 1H, ArH), 7.06–7.09 (m, 1H, ArH), 6.89–6.912 (d, J = 8.76 Hz, 1H, ArH), 5.61–5.623 (d, J = 5.08 Hz, 1H, CHN=C*H*Ar), 5.31–5.323 (J = 5.08 Hz, 1H, N=C—C*H* = CH), 5.22 (s, 2H, NCH_2C=O), 3.71 (s, 3H, OCH_3), 3.69 (s, 3H, OCH_3) ppm; ^{13}C NMR (100 MHz, DMSO-d_6): δ = 164.7, 154.7, 151.4, 150.8, 149.0, 145.4, 143.4, 135.2, 133.5, 133.0, 132.9, 131.4, 130.1, 127.1, 124.4, 122.2, 115.4, 112.5, 111.5, 104.7, 56.2, 55.8, 45.8 ppm. ESI-MS *m/z*: 443.6 $[M+H]^+$. Anal. Calcd

for $C_{25}H_{22}N_4O_4$: C, 67.86; H, 5.01; N, 12.66; Found: C, 67.88; H, 5.02; N, 12.67.

4.1.8.7. (*Z*)-2-(6,7-Dimethoxy-2-oxo-3-(2-(pyridin-4-yl)vinyl) quinoxalin-1(2*H*)-yl)-*N*-phenylacetamide (8g). Light red powder 0.23 g (76%); mp = 215–216 °C, ^{1}H NMR (300 MHz, DMSO-d_6): δ = 10.47 (s, 1H, ArNHC=O), 8.73–8.751 (d, J = 6.3 Hz, 2H, ArH), 7.96–8.01 (m, 4H, ArH), 7.60–7.626 (d, J = 7.8 Hz, 2H, ArH), 7.30–7.36 (m, 3H, ArH), 7.09–7.102 (d, J = 3.6 Hz, 2H, ArH), 5.60–5.617 (d, J = 5.08 Hz, 1H, CHN=C*H*Ar), 5.31–5.327 (J = 5.08 Hz, 1H, N=C–C*H*N=CH), 5.21 (s, 2H, NCH_2C=O), 3.90 (s, 3H, OCH_3), 3.89 (s, 3H, OCH_3) ppm; ^{13}C NMR (75 MHz, DMSO-d_6): δ = 165.2, 157.7, 145.6, 151.1, 149.9, 139.1, 133.4, 132.4, 130.5, 129.6, 128.0, 124.1, 123.0, 121.6, 119.6, 109.7, 69.4, 56.2, 55.1 ppm. ESI-MS m/z: 443.8 $[M+H]^+$. Anal. Calcd for $C_{25}H_{22}N_4O_4$: C, 67.86; H, 5.01; N, 12.66; Found: C, 67.85; H, 5.03; N, 12.68.

4.1.9. General procedure for *N*-(4-substitutedphenyl)-2-((3-methylquinoxalin-2-yl)oxy)acetamide (9a–b)

In a round-bottom flask, compound **6a** (2 mmol) was dissolved in 20 mL of anhydrous dichloromethane at 0 °C. Then isobutyl chloroformate (2.4 mmol, 1.2 equiv) and 4-methylmorpholine (2.4 mmol, 1.2 equiv) were successively added and the resulting solution was stirred in an ice-salt baths for 30 min. The ice-salt bath was then removed and appropriate aniline (2.4 mmol, 1.2 equiv) was added, the mixture was then allowed to react at room temperature under nitrogen atmosphere for about 3–4 h until the completion of reaction. The reaction mixture was diluted with distilled water and extracted with CH_2Cl_2 (3 × 20 mL), the combined organic phase was successively washed with 5% $KHSO_4$, saturated Na_2CO_3, water, and brine, then dried over anhydrous $MgSO_4$. After filtration and concentration in vacuo, the obtained residue was purified by flash chromatography (PE/EtOAc = 4:1, v:v) to afford the desired products.

4.1.9.1. 2-((3-Methylquinoxalin-2-yl)oxy)-*N*-(*p*-tolyl)acetamide (9a). Off-white powder 0.39 g, yield: 64%; ^{1}H NMR (300 MHz, DMSO-d_6): δ = 10.32 (s, 1H, ArNHC=O), 7.94–7.96 (m, 2H, ArH), 7.74–7.76 (m, 2H, ArH), 7.48–7.54 (m, 2H, ArH), 7.28–7.31 (m, 2H, ArH), 5.15 (s, 2H, NCH_2C=O), 2.67 (s, 3H, $ArCH_3$), 2.47 (s, 3H, N=CCH_3) ppm; ESI-MS m/z: 308.5 $[M+H]^+$. Anal. Calcd for $C_{18}H_{17}N_3O_2$: C, 70.34; H, 5.58; N, 13.67; Found: C, 70.33; H, 5.56; N, 13.68.

4.1.9.2. *N*-(4-Chlorophenyl)-2-((3-methylquinoxalin-2-yl)oxy) acetamide (9b). White powder 0.33 g, yield: 51%; ^{1}H NMR (300 MHz, DMSO-d_6): δ = 10.32 (s, 1H, ArNHC=O), 7.93–7.95 (m, 2H, ArH), 7.72–7.75 (m, 2H, ArH), 7.38–7.40 (m, 2H, ArH), 7.30–7.33 (m, 2H, ArH), 5.15 (s, 2H, NCH_2C=O), 2.45 (s, 3H, N=CCH_3) ppm; ESI-MS m/z: 328.8 $[M+H]^+$. Anal. Calcd for $C_{17}H_{14}ClN_3O_2$: C, 62.30; H, 4.31; N, 12.82; Found: C, 62.31; H, 4.33; N, 12.81.

4.1.10. General procedure for (*Z*)-*N*-(4-substitutedphenyl)-2-((3-(2-(pyridin-4-yl)vinyl)quinoxalin-2-yl)oxy)acetamide (10a–b)

The synthetic procedure of compounds **10a**–**b** was similar with that of compounds (**8a**–**g**).

4.1.10.1. (*Z*)-2-((3-(2-(Pyridin-4-yl)vinyl)quinoxalin-2-yl)oxy)-*N*-(*p*-tolyl)acetamide (10a). Light yellow crystal 0.22 g (52%); mp = 179–180 °C; ^{1}H NMR (300 MHz, DMSO-d_6): δ = 10.11 (s, 1H, ArNHC=O), 8.49–8.51 (m, 2H, ArH), 7.80–7.93 (dd, J_1 = 7.8 Hz, J_2 = 0.9 Hz, 1H, ArH), 7.75–7.78 (m, 1H, ArH), 7.69–7.71 (m, 1H, ArH), 7.60–7.62 (m, 1H, ArH), 7.48–7.508 (d, J = 8.4 Hz, 2H, ArH), 7.43 (d, J = 6.0 Hz, 2H, ArH), 7.12–7.148 (d, J = 8.4 Hz, 2H, ArH), 5.74–5.758 (d, J = 5.4 Hz, 1H, CHN=C*H*Ar), 5.25–5.27 (d, J = 5.4 Hz, 1H, N=C–C*H*N=CH), 5.19–5.24 (d, J = 15 Hz, 1H, NCH_2C=O), 2.25 (s, 3H, $ArCH_3$) ppm; ^{13}C NMR (75 MHz, DMSO-d_6): δ = 166.1, 155.5, 154.5, 149.9, 148.5, 139.2, 138.8, 136.4, 133.0, 130.1, 129.7, 128.6, 127.5, 127.0, 121.5, 120.0, 70.0, 65.0, 20.9 ppm. ESI-MS m/z: 414.6 $[M+NH_4]^+$. Anal. Calcd for $C_{24}H_{20}N_4O_2$: C, 72.71; H, 5.08; N, 14.13; Found: C, 72.73; H, 5.09; N, 14.12.

4.1.10.2. (*Z*)-*N*-(4-Chlorophenyl)-2-((3-(2-(pyridin-4-yl)vinyl) quinoxalin-2-yl)oxy)acetamide (10b). White crystal 0.13 g (67%); mp = 218–219 °C; ^{1}H NMR (300 MHz, DMSO-d_6): δ = 10.36 (s, 1H, ArNHC=O), 8.50–8.52 (m, 3H, ArH), 7.75 (m, 5H, ArH), 7.44 (m, 4H, ArH), 5.75–5.768 (d, J = 5.4 Hz, 1H, CHN=C*H*Ar), 5.38–5.398 (d, J = 5.4 Hz, 1H, N=C–C*H*N=CH), 5.16–5.209 (d, J = 14.7 Hz, 1H, NCH_2C=O), 2.26 (s, 3H, $ArCH_3$) ppm; ^{13}C NMR (75 MHz, DMSO-d_6): δ = 166.1, 154.9, 154.0, 149.4, 147.9, 138.7, 138.3, 137.4, 129.6, 128.7, 128.1, 127.2, 127.0, 126.5, 121.0, 120.9, 69.4, 64.5 ppm; ESI-MS m/z: 434.7 $[M+H]^+$. Anal. Calcd for $C_{23}H_{17}ClN_4O_2$: C, 66.27; H, 4.11; N, 13.44; Found: C, 66.28; H, 4.09; N, 13.45.

4.1.11. Methyl 4-(bromomethyl)benzoate (11)

In a round-bottom flask, 4-(bromomethyl)benzoic acid (3.4 g, 20 mmol) was dissolved in 50 mL of anhydrous methanol at 0 °C. After being stirred for 10 min, 40 mL of acetyl chloride was added dropwise to the above mixture and continued to react for 15 min. Then the ice-bath was removed and the reaction mixture was heated to 70 °C and reacted for additional 6 h. The mixture was concentrated in vacuo and afforded the desired product as oil which was used directly without any further purification.

4.1.12. Methyl 4-((3-methyl-2-oxoquinoxalin-1(2*H*)-yl)methyl) benzoate (12)

A round-bottom flask charged with 3-methylquinoxalin-2(1*H*)-one (compound **2a**, 1.6 g, 10 mmol), K_2CO_3 (1.7 g, 12 mmol), and KI (170 mg, 1 mmol), 30 mL of acetone was then added. The resulting suspension was added compound **11** (1.84 g, 12 mmol) dropwise and then flushed with nitrogen gas. After heating and reacting at 62 °C for 8 h under nitrogen atmosphere, the solvent was removed under reduced pressure. The residue was extracted with ethyl acetate (3 × 20 mL), washed with water and brine, and dried over anhydrous $MgSO_4$. Filtration and concentration in vacuo afforded the crude product which was purified by chromatography column (PE: EtOAc = 8:1, v:v) to afford 2.4 g (71%) of pure product as white crystal. ESI-MS m/z: 309.5 $[M+H]^+$, 331.4 $[M+Na]^+$. Anal. Calcd for $C_{18}H_{16}N_2O_3$: C, 70.12; H, 5.23; N, 9.09; Found: C, 70.13; H, 5.22; N, 9.08.

4.1.13. 4-((3-Methyl-2-oxoquinoxalin-1(2*H*)-yl)methyl)benzoic acid (13)

Compound **12** (1.54 g, 5 mmol) and KOH (0.34 g, 6 mmol) was suspended in 50% ethanol solution (40 mL), the resulting solution was reacted at room temperature for 3 h. The organic solvent was removed in vacuo and the resulting water phase was washed with EtOAc (10 mL), the combined water was acidified by 1 N HCl until a large amount of white solid was precipitated. Filtered and recrystallized with 70% methanol to give the pure product 1.38 g (94%) as white solid. Mp: 211–212 °C, ESI-MS m/z: 293.6 $[M-H]^-$. Anal. Calcd for $C_{17}H_{14}N_2O_3$: C, 69.38; H, 4.79; N, 9.52; Found: C, 69.37; H, 4.77; N, 9.54.

4.1.14. General synthetic protocol for 4-substituted-*N*-(4-((3-methyl-2-oxoquinoxalin-1(2*H*)-yl)methyl)phenyl)benzamide (15)

To a solution of compound **13** (0.3 g, 1.1 mmol) in 20 mL of dioxane was added successively DPPA (330 mg, 1.2 mmol) and triethylamine (120 mg, 1.2 mmol). The resulting solution was

heated to 110 °C and refluxed at the same temperature for 6 h. Then the reaction was cooled to room temperature and added appropriate substituted phenylamines (1.2 mmol, 1.1 equiv). The mixture was then stirred at rt for additional 12 h. After completion of the reaction, it was quenched with distilled water (20 mL). The obtained suspension was diluted with EtOAc (30 mL) and washed with water and brine, and dried over anhydrous Na_2SO_4. The residue was purified by flash chromatography (PE:EtOAc = 5:1, v:v) to afford the desired amide products. One thing to note here is that if the solvent dioxane was changed into other solvents with higher boiling point (e.g., toluene), the urea products rather than amide compounds will be generated, which is on-going in our lab.

4.1.14.1. 4-Methyl-*N*-(4-((3-methyl-2-oxoquinoxalin-1(2*H*)-yl) methyl)phenyl)benzamide (15a). White solid (0.31 g, 71%); mp = 242–243 °C; ^{1}H NMR (400 MHz, DMSO-d_6): δ = 10.11 (s, 1H, ArNHC=O), 7.85–7.87 (m, 2H, ArH), 7.78–7.80 (d, J = 8.0 Hz, 1H, ArH), 7.61–7.631 (d, J = 8.4 Hz, 2H, ArH), 7.32–7.48 (m, 5H, ArH), 7.12–7.14 (m, 2H, ArH), 5.58 (s, 2H, NCH_2C=O), 2.53 (s, 3H, Ar CH_3), 2.26 (s, 3H, N=CCH_3) ppm; ^{13}C NMR (100 MHz, DMSO-d_6): δ = 165.5, 158.5, 155.1, 140.0, 137.1, 134.7, 133.1, 132.8, 130.0, 129.4, 128.5, 127.2, 124.0, 120.8, 115.4, 45.2, 21.8, 20.9 ppm; ESI-MS m/z: 384.7 $[M+H]^+$. Anal. Calcd for $C_{24}H_{21}N_3O_2$: C, 75.18; H, 5.52; N, 10.96; Found: C, 75.17; H, 5.54; N, 10.94.

4.1.14.2. 4-Chloro-*N*-(4-((3-methyl-2-oxoquinoxalin-1(2*H*)-yl) methyl)phenyl)benzamide (15b). White solid (0.28 g, 63%); mp = 254–255 °C; ^{1}H NMR (400 MHz, DMSO-d_6): δ = 10.32 (s, 1H, ArNHC=O), 7.77–7.80 (m, 2H, ArH), 7.76–7.78 (m, 3H, ArH), 7.46–7.50 (m, 1H, ArH), 7.31–7.42 (m, 6H, ArH), 5.56 (s, 2H, NCH_2 C=O), 2.53 (s, 3H, N=CCH_3) ppm; ^{13}C NMR (100 MHz, DMSO-d_6): δ = 165.8, 158.5, 155.1, 140.2, 138.6, 134.4, 132.8, 132.7, 130.0, 129.4, 129.0, 128.6, 127.7, 127.3, 124.0, 122.2, 115.4, 45.2, 21.8 ppm; ESI-MS m/z: 404.8 $[M+H]^+$. Anal. Calcd for $C_{23}H_{18}ClN_3O_2$: C, 68.40; H, 4.49; Cl, 8.78; N, 10.40; Found: C, 68.41; H, 4.50; Cl, 8.77, N, 10.41.

4.2. Biological protocols

4.2.1. In vitro antiproliferative assay

The in vitro cytotoxicity of test compounds was determined by evaluating the growth inhibition rates on certain concentrations by MTT (3-[4,5-dimethyl-2-thiazolyl]-2,5-diphenyl-2*H*-tetrazolium bromide) method. In brief, tumor cells were plated in a 96-well plate (8000 cells per well) in RPMI-1640 culture medium with 10% (v/v) heat-inactivated fetal bovine serum (FBS), and allowed to adhere and spread for 10 h. Then the culture medium was removed and 100 μg/mL of positive control drug, test compounds in RPMI-1640 culture medium with 1% FBS (with 0.1% DMSO as fluxing agent, also in the control the zero-setting wells) were added, and then the cells were cultured for 24 h at 37 °C in a CO_2 incubator. MTT solution (10 μL of 5 mg/mL) was added per well and the cells were cultured for additional 4 h. The blue formazan crystals formed from MTT was pelleted to the bottom of well by centrifugation, then adding 100 μL of DMSO per well and mixing for another 15 min. The optical density (OD) values were measured at 590 nm. The growth inhibition rate was calculated as $[(OD_c - OD_t)/(OD_c - OD_z)] \times 100$. OD_c represents the OD values of the control group, OD_t represents the OD values of the treating groups, and OD_z represents the OD values of the zero-setting groups. Two separate experiments with triplicate data were performed to achieve the cytotoxic results, and the IC_{50} values were calculated according to the inhibition ratios.

4.2.2. Tubular structure formation assay in HUVEC

Before the HUVEC tubular structure formation assay, Matrigel (BD Bioscience, Bedford, MA) was polymerized in 24-well plates at 37 °C for 1 h. Then HUVEC was trypsinized and seeded onto Matrigel at a concentration of 10^5 cells per well and then incubated with various concentration of Pazopanib or test compounds (0.1, 1, and 10 μg/mL) for 8 h at 37 °C in a CO_2 incubator until the tube network formed. Cellular morphology was then taken under a microscope (OLYMPUS IX51) in five random fields per well at a four magnification. Experiment was repeated 3 times.

4.2.3. Ex vivo antiangiogenic assay in rat aortic ring

The aortas were harvested from 6-week-old Sprague–Dawley rats. Each aorta was cut into 1-mm slices and embedded in 70 μL Matrigel in 96-well plates. The aortic rings were then fed with 100 μL of RPMI-1640 culture medium without FBS (with 0.1% DMSO in final concentration) with or without different concentrations of Pazopanib or test compounds (0.1 μg/mL), and photographed on the 6th day. The quantity of microvessels is valued by relative area covered with microvessels using Image-Pro Express.

4.2.4. In vivo antiangiogenic assay in zebrafish model

Two zebrafish types were used as the in vivo model, they are the transgenic zebrafish Tg(*flk1*:GFP) which express strong green fluorescent protein (GFP) in their endothelial cell and also the wild-type zebrafish. Both of them were kindly donated by Prof Jianfeng Zhou from Ocean University of China. Both stocks were maintained as described in the zebrafish handbook and all animal experiments were performed in accordance with the ethical guidelines of the Shandong University. In brief, stocks were maintained in a controlled environment at a temperature of 28 °C on 1 14 h:10 h light:dark cycle. The fish were fed twice daily with artemia nauplii in the morning and afternoon, and occasionally with general tropical fish food. The embryos were collected in the morning and cultured at 28 °C in embryo medium. One day after fertilization, the embryos were dechorionated with tweezers in a 12-well plate coated with 1% agarose and distributed into per well with 3 mL of assay solution. The embryos receiving a solution of DMSO (0.2%) was utilized as the vehicle-treated control and the concentrations of test compounds were prepared as 10, 50, and 100 μM. All the experiments were repeated at least three times, with 10 embryos per well. Before the assay, the embryos that have precultured with embryo rearing solution (ERS) were treated with 0.1% methylenedi, and for the transgenic group, 0.1% *N*-phenylthiourea (PTU) was supplemented. After treatment with the compound for 24 h, the embryos were observed for morphological changes using an Olympus Spinning Disk Confocal Microscope System (Nikon SMZ1500) at 50- and 100-fold magnification, respectively.

4.2.5. Kinase inhibition assay

The ability of compounds to inhibit the phosphorylation of a peptide substrate by the recombinant human enzymes (Sigma) was evaluated in a microtiter plate format using luciferase analysis. Briefly, 15 μL of reaction mixture containing the kinase reaction buffer (40 mM Tris, pH 7.4; 10 mM $MgCl_2$; 0.1 mg/mL BSA; 1 mM DTT; 10 μM ATP) and kinase substrate was incubated at 30 °C for 5 min in 96-well microtiter plates. After addition of specific kinase, the samples (final volume of 50 μL) were incubated for further 50 min in the absence (control) or in the presence of different concentrations of test compounds and during incubation the fluorescence intensity (λ_{ex} = 355 nm, λ_{em} = 460 nm) was recorded on a MD-SpectraMax M5 microplate reader. % activity = {(Lu no kinase − Lu compound)/(Lu no kinase − Lu kinase)} × 100%.

4.3. Statistical analysis

Experimental values were expressed as mean ± SD. Statistical analysis was performed with two-tailed Student's *t*-test or Mann–Whitney test using Prism 6.0 (GraphPad Software, Inc., San Diego, CA). A *P*-value <0.05 was considered statistically significant.

4.4. Molecular modeling study

AutoDock 4.2 program was used to simulate a binding model by docking into the active site of VEGFR-2 (PDB code: 3EWH), and the docking study was performed roughly as follows. (1) *Protein template preparation:* X-ray crystal structure of VEGFR-2 was downloaded from RCSB. Two missing loops, Asp857-Thr861 and Arg1051-Asp1056, were reconstructed by SuperLooper web server. The energy of reconstructed template was minimized by MOE using AMBER94 force field. Nonpolar hydrogens of new template 3EWHOK were merged before adding Gasteiger Huckel charges by AutoDockTools (ADT) 1.5.2. After that, types of atoms were assigned and grid representation of 3EWHOK was prepared by AutoGrid4. (2) *Ligand preparation:* compound **8c** was optimized with Chem3D Ultra 12.0. Ligands AAX, GIG, K11, LIF, 877 and 900 were extracted from crystal poses. These ligands were prepared with ADT1.5.2 as follow: Gasteiger charges were assigned, nonpolar hydrogens were merged, aromatic carbons were identified, and the rigid root and rotatable bonds were defined. (3) *Docking procedures:* The docking simulations were performed using the Lamarckian genetic algorithm (LGA) with 100 solutions for each ligand obtained, in which the default values of the other parameters were used. The binding model with the lowest binding free energy for each inhibitor is selected as the best model.

Acknowledgments

This work was partially supported by the Natural Science Foundation of Shandong Province (No. ZR2013HM101), Program for Changjiang Scholars and Innovative Research Team in University (PCSIRT, No. IRT13028) and China–Australia Centre for Health Sciences Research Program (No. 2015GJ07). Ms. Ying Feng has contributed a lot for the in vivo zebrafish assay, and Dr. Qiang Wang's helpful discussion with regard to the docking study is also appreciated.

References and notes

1. Lv, Y. C.; Li, M. Y.; Liu, T.; Tong, L. J.; Peng, T.; Wei, L. X.; Ding, J.; Xie, H.; Duan, W. H. *ACS Med. Chem. Lett.* **2014**, *5*, 592.
2. Abdel-Rahman, O. *Crit. Rev. Oncol. Hemat.* **2015**, *93*, 18.
3. Musumeci, F.; Radi, M.; Brullo, C.; Schenone, S. *J. Med. Chem.* **2012**, *55*, 10797.
4. Eskander, R. N.; Tewari, K. S. *Gynecol. Oncol.* **2014**, *132*, 496.
5. Shi, L. L.; Zhou, H.; Wu, J. F.; Li, X. *Mini Rev. Org. Chem.* **2015**, *12*, 96.
6. Li, Y. G.; Zhang, J.; Xu, W. F.; Zhu, H. W.; Li, X. *Bioorg. Med. Chem.* **2010**, *18*, 1516.
7. Yuan, H. Y.; Li, X.; Qu, X. J.; Sun, L. R.; Xu, W. F.; Tang, W. *Med. Chem. Res.* **2009**, *18*, 671.
8. Zakharia, Y.; Zakharia, K.; Rixe, O. *Expert Opin. Drug Disc.* **2015**, *10*, 925.
9. Pemovska, T.; Johnson, E.; Kontro, M.; Repasky, G. A.; Chen, J.; Wells, P.; Cronin, C. N.; McTigue, M.; Kallioniemi, O.; Porkka, K.; Murray, B. W.; Wennerberg, K. *Nature* **2015**, *519*, 102.
10. Escudier, B.; Gore, M. *Drugs R. D.* **2011**, *11*, 113.
11. Gaumann, A. K.; Drexler, H. C.; Lang, S. A.; Stoeltzing, O.; Diermeier-Daucher, S.; Buchdunger, E.; Wood, J.; Bold, G.; Breier, G. *Int. J. Oncol.* **2014**, *45*, 2267.
12. Dragovich, T.; Laheru, D.; Dayyani, F.; Bolejack, V.; Smith, L.; Seng, J.; Burris, H.; Rosen, P.; Hidalgo, M.; Ritch, P.; Baker, A. F.; Raghunand, N.; Crowley, J.; Von Hoff, D. D. *Cancer Chemother. Pharmacol.* **2014**, *74*, 379.
13. To, K. K.; Poon, D. C.; Wei, Y.; Wang, F.; Lin, G.; Fu, L. W. *Biochem. Pharmacol.* **2015**, *97*, 27.
14. Bold, G.; Altmann, K. H.; Frei, J.; Lang, M.; Manley, P. W.; Traxler, P.; Wietfeld, B.; Brüggen, J.; Buchdunger, E.; Cozens, R.; Ferrari, S.; Furet, P.; Hofmann, F.; Martiny-Baron, G.; Mestan, J.; Rösel, J.; Sills, M.; Stover, D.; Acemoglu, F.; Boss, E.; Emmenegger, R.; Lässer, L.; Masso, E.; Roth, R.; Schlachter, C.; Vetterli, W. *J. Med. Chem.* **2000**, *43*, 2310.
15. Potashman, M. H.; Bready, J.; Coxon, A., Jr.; DeMelfi, T. M.; DiPietro, L.; Doerr, N.; Elbaum, D.; Estrada, J.; Gallant, P.; Germain, J.; Gu, Y.; Harmange, J. C.; Kaufman, S. A.; Kendall, R.; Kim, J. L.; Kumar, G. N.; Long, A. M.; Neervannan, S.; Patel, V. F.; Polverino, A.; Rose, P.; Plas, Sv.; Whittington, D.; Zanon, R.; Zhao, H. *J. Med. Chem.* **2007**, *50*, 4351.
16. Su, P.; Wang, J.; Shi, Y.; Pan, X.; Shao, R.; Zhang, J. *Bioorg. Med. Chem.* **2015**, *23*, 3228.
17. Wang, C.; Gao, H.; Dong, J.; Zhang, Y.; Su, P.; Shi, Y.; Zhang, J. *Bioorg. Med. Chem.* **2014**, *22*, 277.
18. Quaife, N. M.; Watson, O.; Chico, T. J. *Curr. Opin. Pharmacol.* **2012**, *12*, 608.
19. Cho, Y. S.; Jung, H. G.; Seok, S. H.; Payumo, A. Y.; Chen, J. K.; Kwon, H. J. *Biochem. Biophys. Res. Commun.* **2013**, *433*, 396.
20. Wilhelm, S. M.; Carter, C.; Tang, L.; Wilkie, D.; McNabola, A.; Rong, H.; Chen, C.; Zhang, X.; Vincent, P.; McHugh, M.; Cao, Y.; Shujath, J.; Gawlak, S.; Eveleigh, D.; Rowley, B.; Liu, L.; Adnane, L.; Lynch, M.; Auclair, D.; Taylor, I.; Gedrich, R.; Voznesensky, A.; Riedl, B.; Post, L. E.; Bollag, G.; Trail, P. A. *Cancer Res.* **2004**, *64*, 7099.
21. Yang, W.; Chen, Y.; Zhou, X.; Gu, Y.; Qian, W.; Zhang, F.; Han, W.; Lu, T.; Tang, W. *Eur. J. Med. Chem.* **2015**, *89*, 581.
22. Gao, H.; Su, P.; Shi, Y.; Shen, X.; Zhang, Y.; Dong, J.; Zhang, J. *Eur. J. Med. Chem.* **2015**, *90*, 232.
23. Vijayan, R. S.; He, P.; Modi, V.; Duong-Ly, K. C.; Ma, H.; Peterson, J. R., Jr.; Dunbrack, R. L.; Levy, R. M. *J. Med. Chem.* **2015**, *58*, 466.
24. Shi, L.; Wu, T. T.; Wang, Z.; Xue, J. Y.; Xu, Y. G. *Eur. J. Med. Chem.* **2014**, *84*, 698.
25. Shi, L.; Gao, H.; Dong, J.; Zhang, Y.; Su, P.; Shi, Y.; Zhang, J. *Bioorg. Med. Chem.* **2014**, *22*, 277.